Supplement of Weather Clim. Dynam., 6, 571–594, 2025
https://doi.org/10.5194/wcd-6-571-2025-supplement

Supplement of

Weather type reconstruction using machine learning approaches

Lucas Pfister et al.

Correspondence to: Lucas Pfister (lucas.pfister@unibe.ch)

S1. Predictor correlations

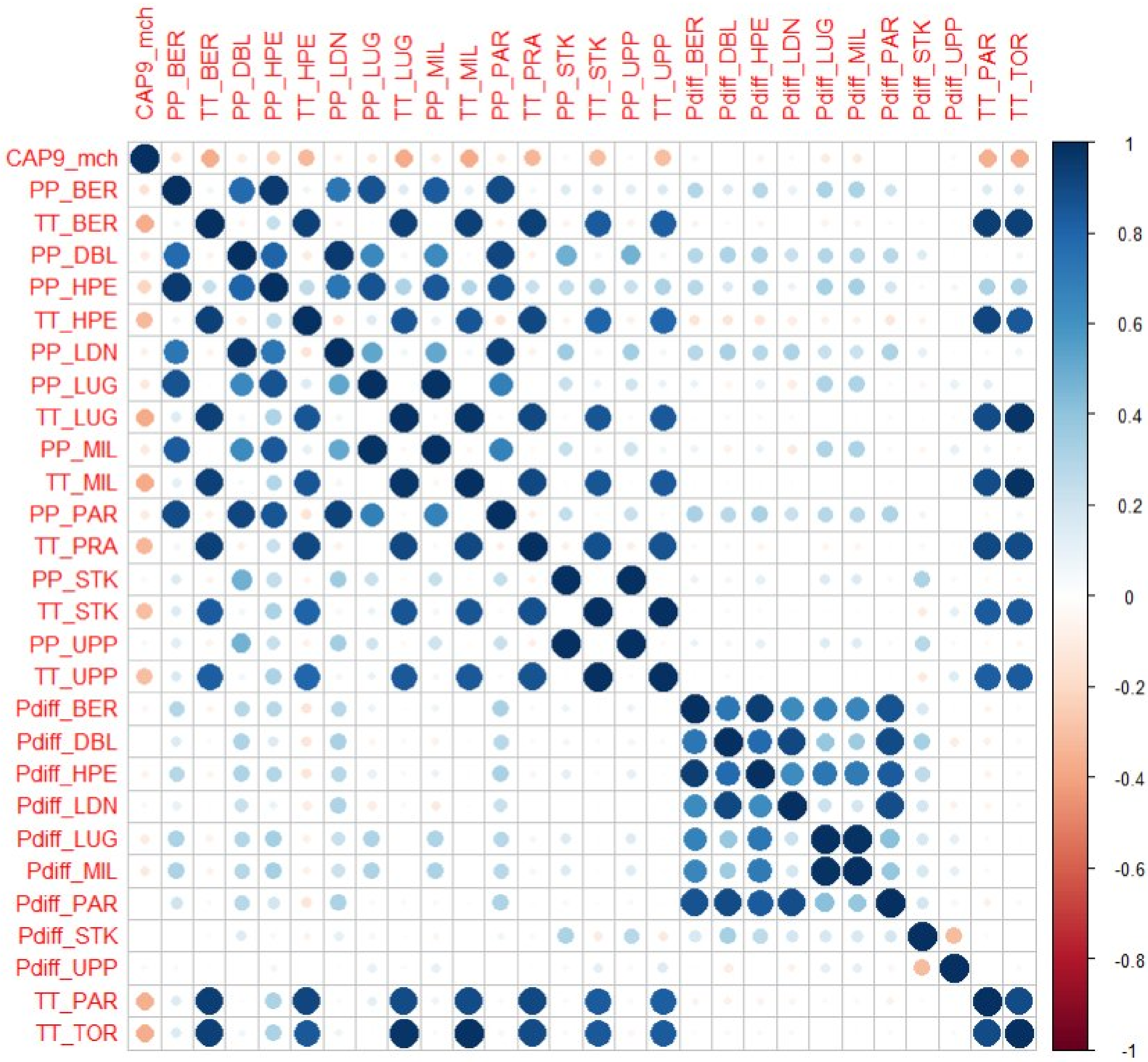

***Figure S1**: Correlations between variables used for the model comparison including the weather types (CAP9_mch). Shown are pearson correlations for the SMD station set with 11 stations as used by Schwander et al. (2017)*

S2. Multinomial logistic regression (MLG) model coefficients and fitted relationships

Table S1: *Coefficients β_n of the six MLG predictands (PP_MIL = sea level pressure Milan, PP_PAR = sea level pressure Paris, TT_PRA = temperature Prague, TT_STK = temperature Stockholm, Pdiff_MIL = pressure gradient Milan and Pdiff_STK = pressure gradient Stockholm) for each CAP9 class. Class one is taken as reference. All predictands are highly significant (not shown).*

Class	**Intercept**	**PP_MIL**	**PP_PAR**	**TT_PRA**	**TT_STK**	**Pdiff_MIL**	**Pdiff_STK**
2	686.3291	-0.0633	-0.6142	0.1239	-0.1066	-0.0765	-0.0810
3	-998.7799	1.0667	-0.0846	-0.0116	-0.0506	-0.0334	-0.0330
4	-1352.5444	0.9168	0.4126	-0.2003	0.1352	0.0356	0.0510
5	-2597.8647	2.0411	0.5076	-0.3536	0.1913	0.0164	0.0499
6	1334.6536	-0.9174	-0.4009	0.0436	-0.0416	-0.0270	-0.0285
7	2034.2208	-0.9707	-1.0427	0.2170	-0.1497	-0.1160	-0.1034
8	-4061.5719	2.9962	0.9768	-0.6759	0.3139	0.0585	0.0834
9	2957.1726	-1.7344	-1.1998	0.2361	-0.1795	-0.0607	-0.0881

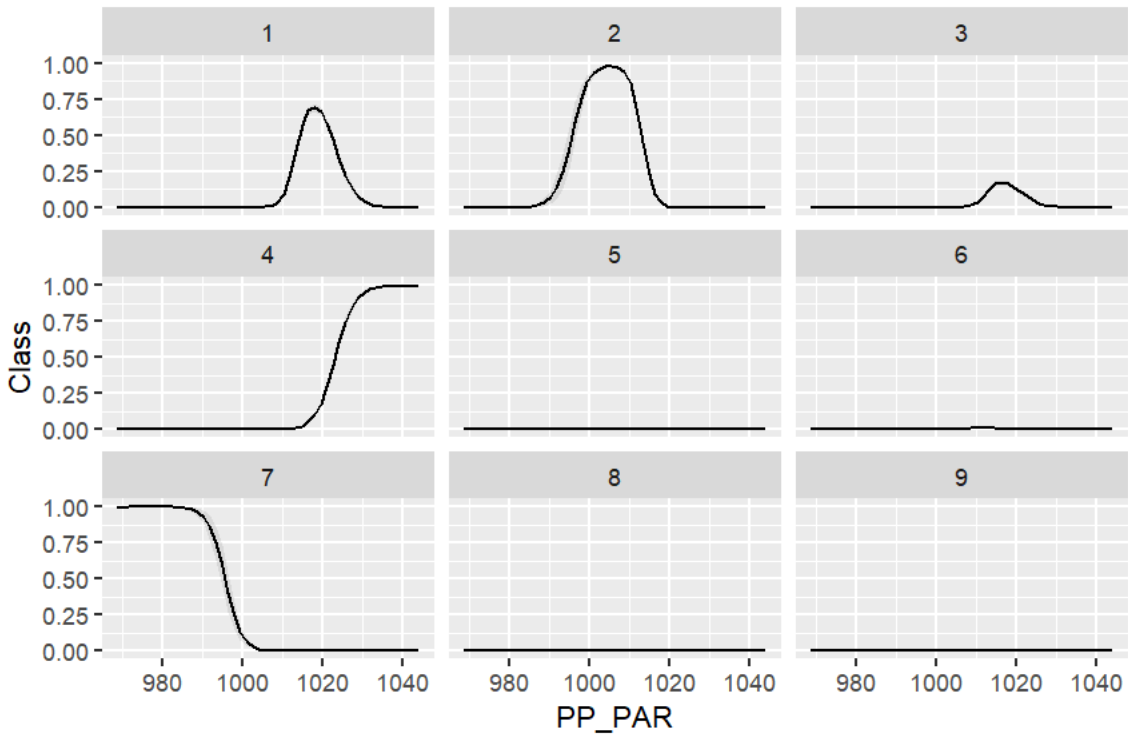

Figure S2: *Fitted model relationships of the predictand PP_PAR per CAP9 class. The probability of the respective class (y-axes) is plotted against the values of PP_PAR in hPa (x-axes).*

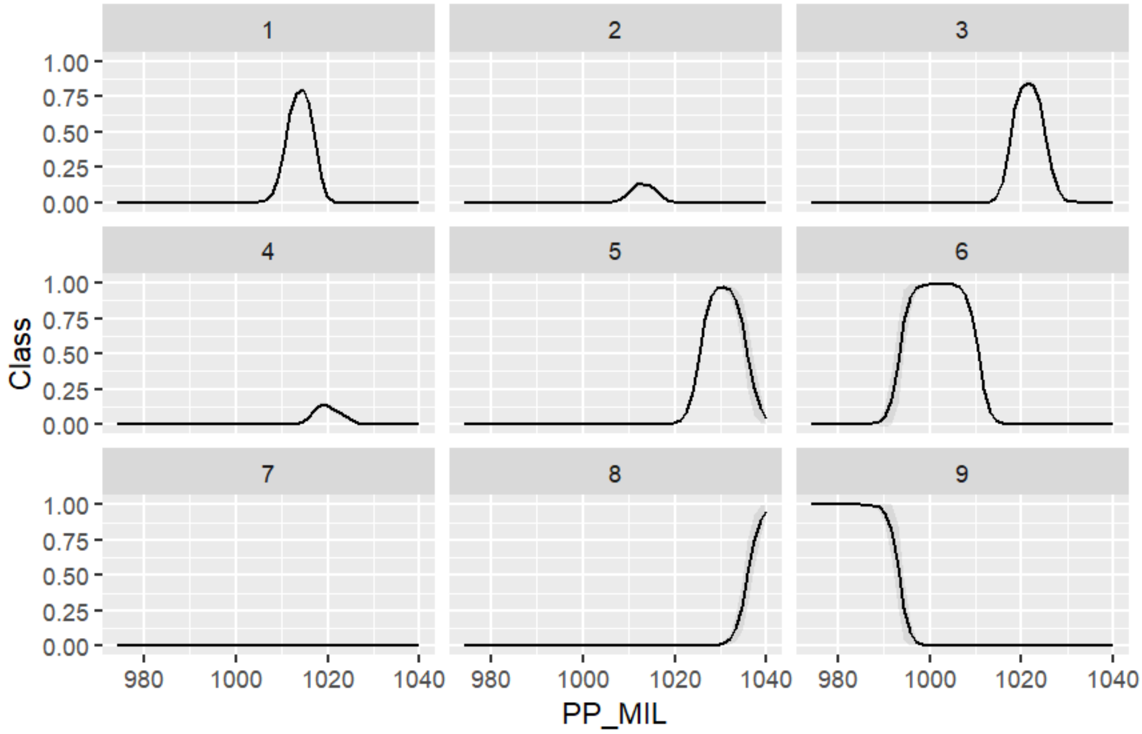

Figure S3*: As figure S2, but for PP_MIL.*

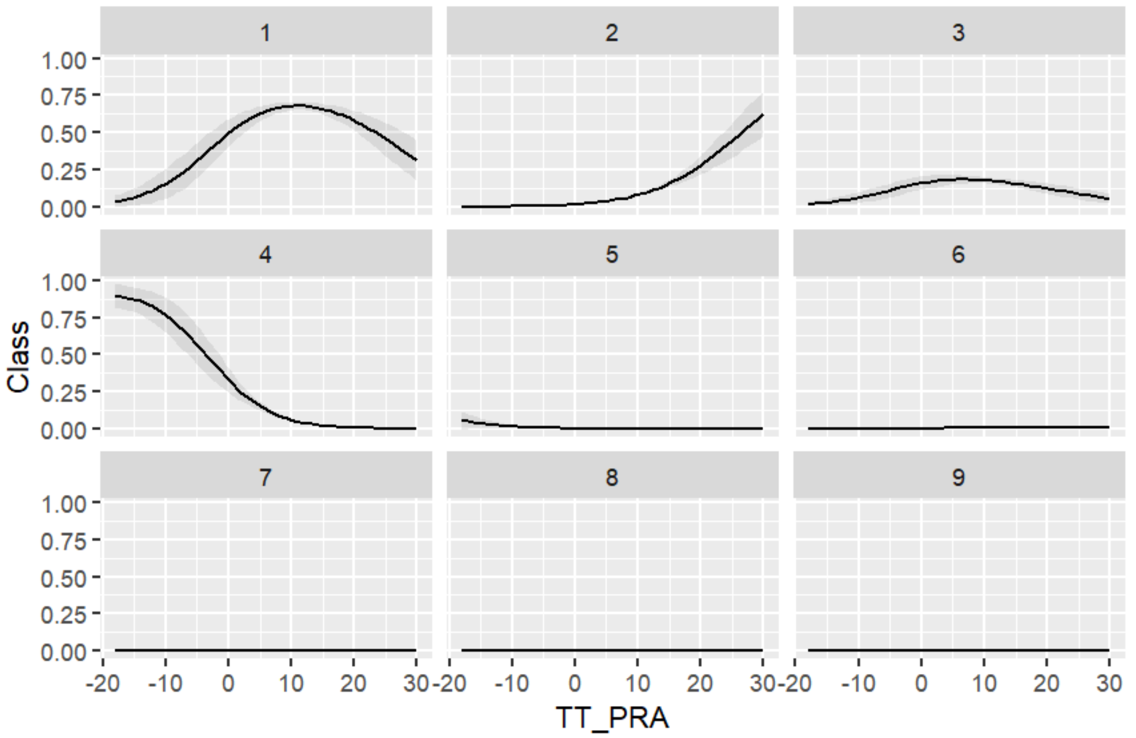

Figure S4*: As figure S2, but for TT_PRA.*

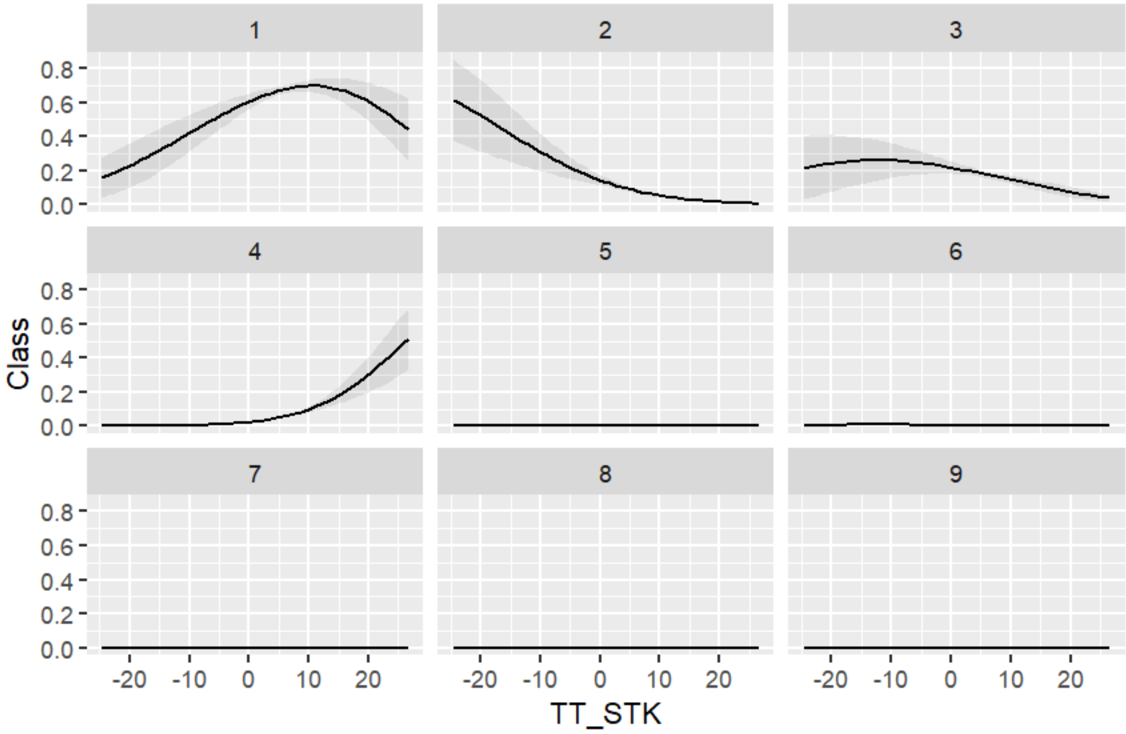

Figure S5: *As figure S2, but for TT_STK.*

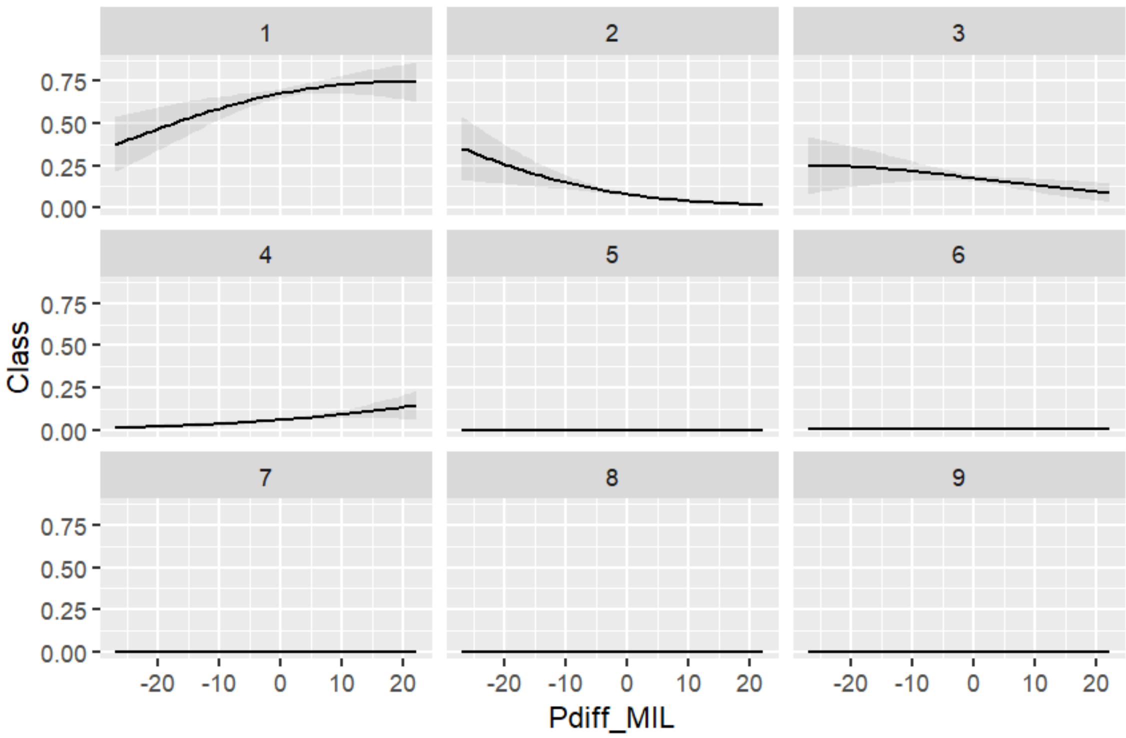

Figure S6: *As figure S2, but for Pdiff_MIL.*

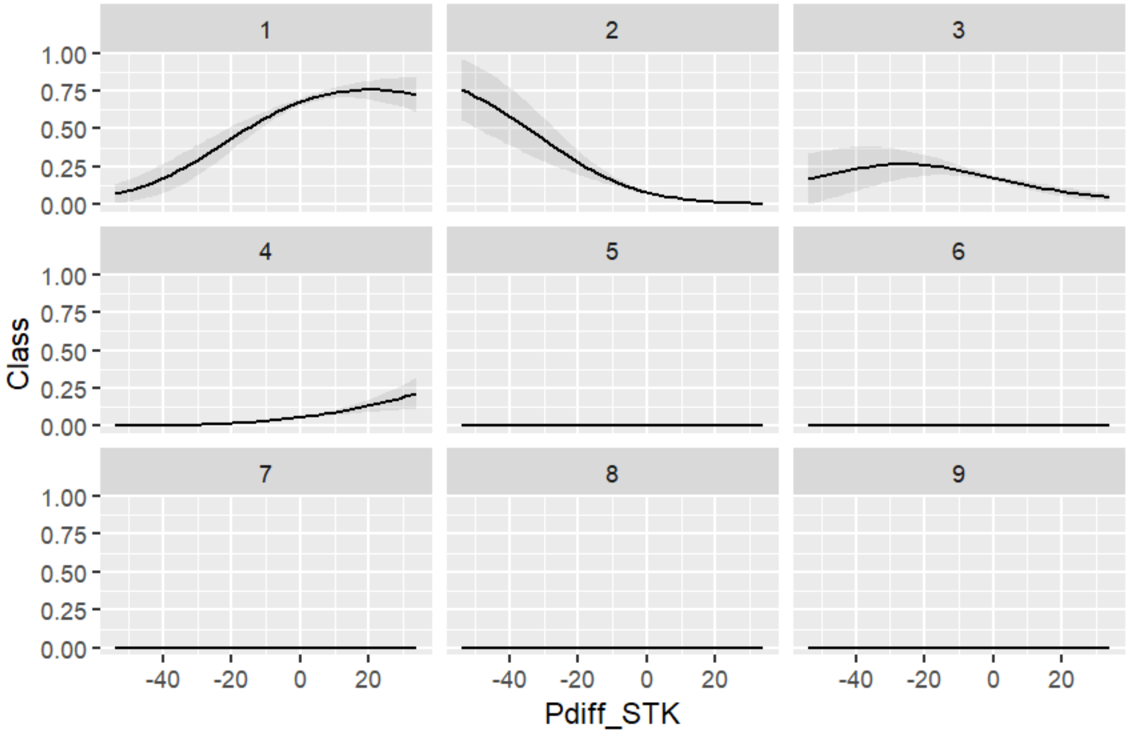

Figure S7: *As figure S2, but for Pdiff_STK.*

S3. Random Forests (RF): Feature Importance

Feature importance (average reduction of the Gini impurity or entropy in the split classes for each feature (predictor) over all trees) of the random forest input data on the example of the SMD stationset with 11 stations as used by Schwander et al. (2017)

input Variable	feature importance	input Variable	feature importance
PP_LUG	0.1580	**TT_SMA**	0.0106
PP_MIL	0.1434	**TT_TOR**	0.0105
PP_DBL	0.1057	**TT_PAR**	0.0093
PP_BAS	0.0811	**TT_UPP**	0.0077
PP_SMA	0.0804	**TT_STK**	0.0075
PP_HPE	0.0712	**Pdiff_DBL**	0.0069
PP_PAR	0.0606	**Pdiff_HPE**	0.0067
PP_BER	0.0473	**Pdiff_STK**	0.0066
PP_LDN	0.0433	**Pdiff_MIL**	0.0065
PP_STK	0.0139	**Pdiff_LDN**	0.0063
PP_UPP	0.0127	**Pdiff_PAR**	0.0063
TT_PRA	0.0119	**Pdiff_BAS**	0.0061
TT_LUG	0.0118	**Pdiff_BER**	0.0059
TT_HPE	0.0117	**Pdiff_LUG**	0.0058
TT_BER	0.0112	**Pdiff_UPP**	0.0058
TT_MIL	0.0110	**Pdiff_SMA**	0.0057
TT_BAS	0.0108		

S4. Neural Network (NN) Architectures

Architectures of the best neural network (NN) models for the input data station sets used for the CAP9 reconstructions. They typically contain between 2 and 5 layers (with between 32 and 224 neurons) and (as predefined) a dropout layer. Input and output layers are shown for completeness. Input layers consist of the preprocessed temperature and pressure series for the given station set. The following flowcharts indicate on the left the layer type (in the terminology of the keras library), the activation function (relu or softmax), and the data format, and on the right the size of the input and output of the respective layers. The dimension 'None' represents the variable time dimension.

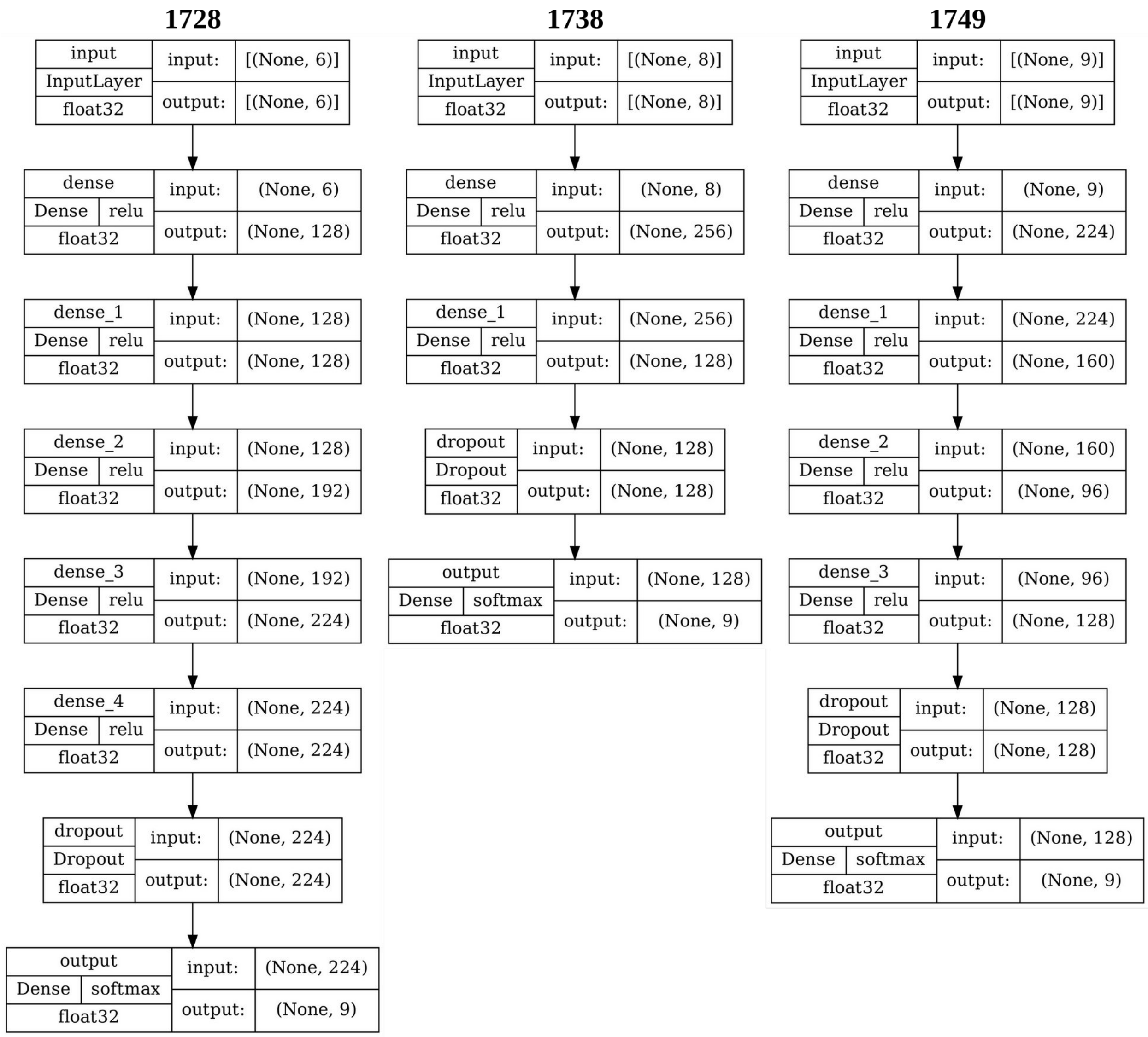

1756

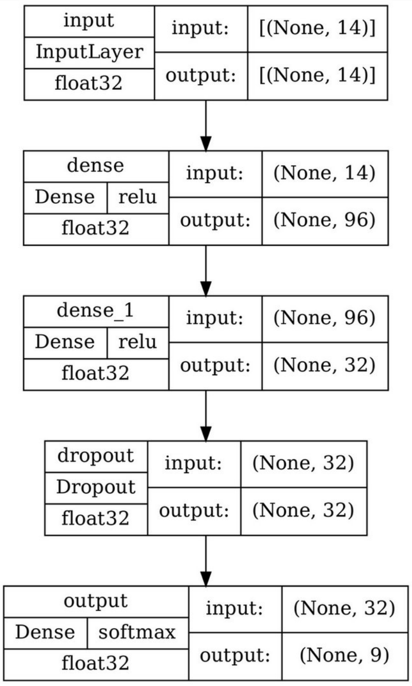

1764

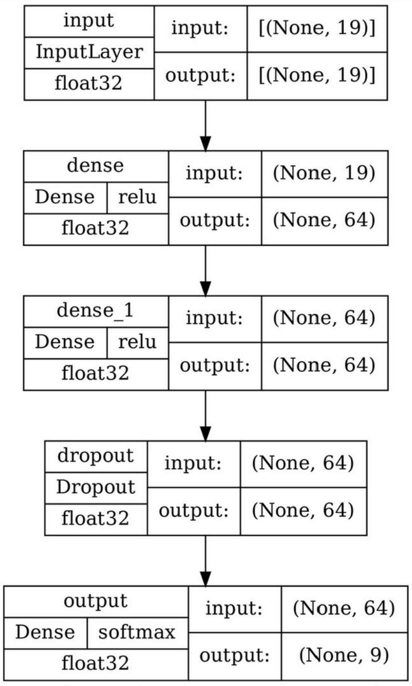

1771

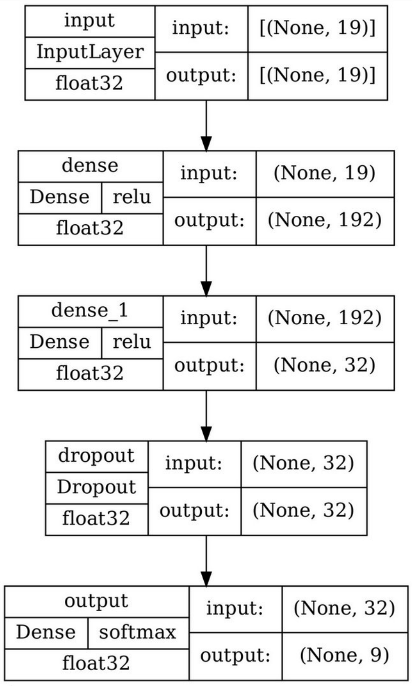

1781

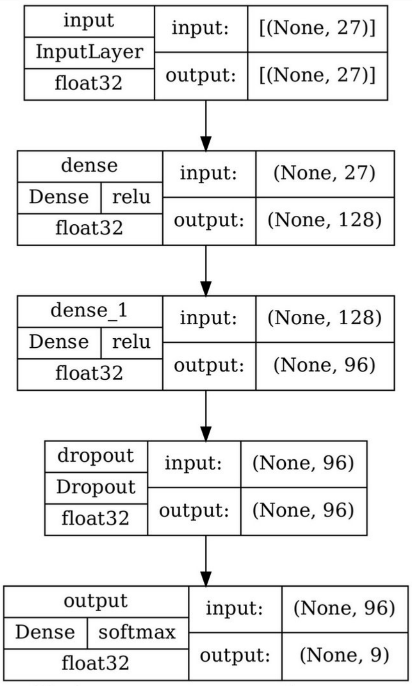

1790

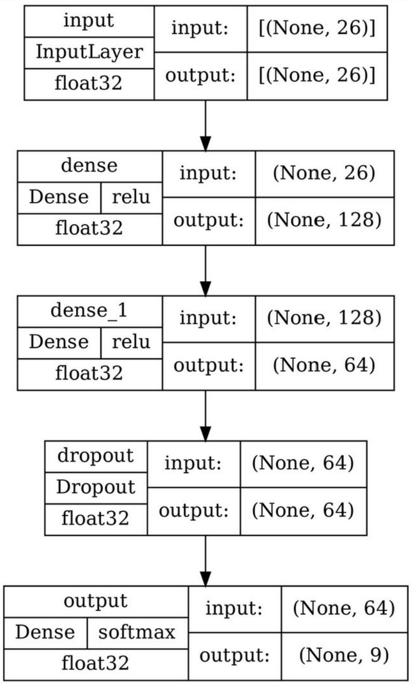

1818

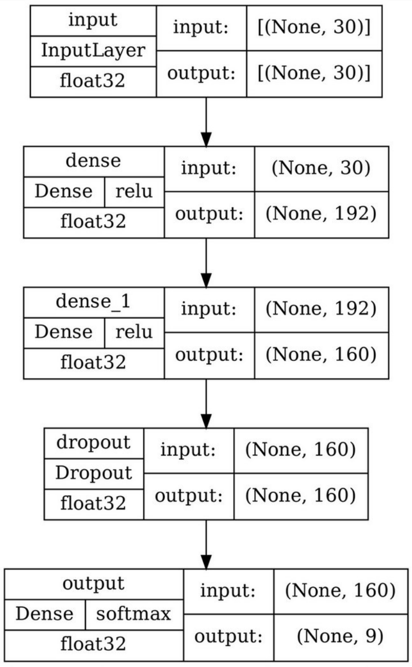

1864

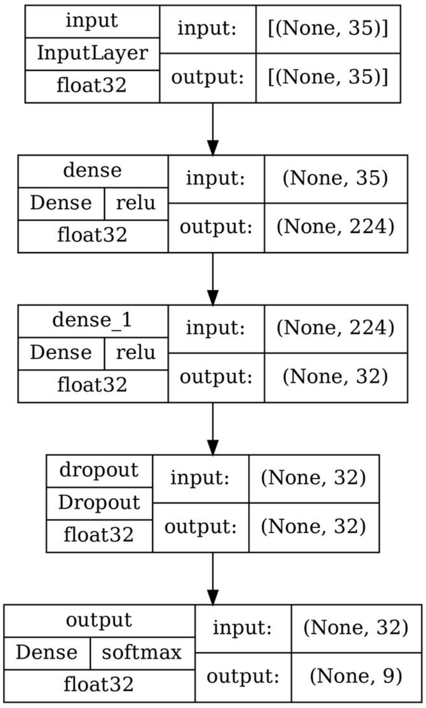

input
InputLayer
float32
input:
[(None, 35)]
output:
[(None, 35)]
dense
Dense
relu
float32
input:
(None, 35)
output:
(None, 224)
dense_1
Dense
relu
float32
input:
(None, 224)
output:
(None, 32)
dropout
Dropout
float32
input:
(None, 32)
output:
(None, 32)
output
Dense
softmax
float32
input:
(None, 32)
output:
(None, 9)

S5. Additional Analyses of CAP9 Reconstructions

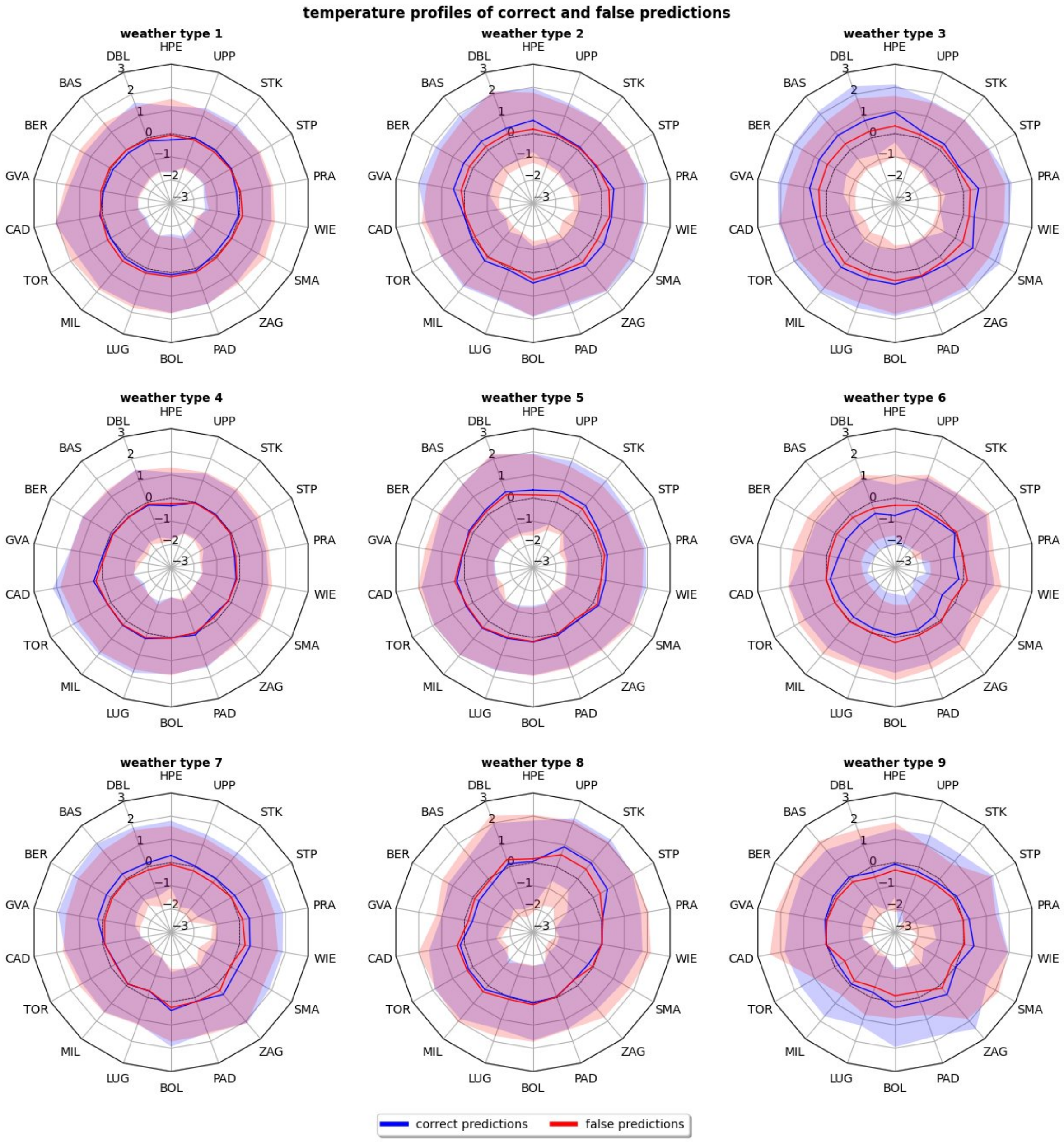

Figure S8: *station observation profiles in standard deviations for correctly and wrongly predicted CAP9 weather types as in Fig. 4, but for temperature.*

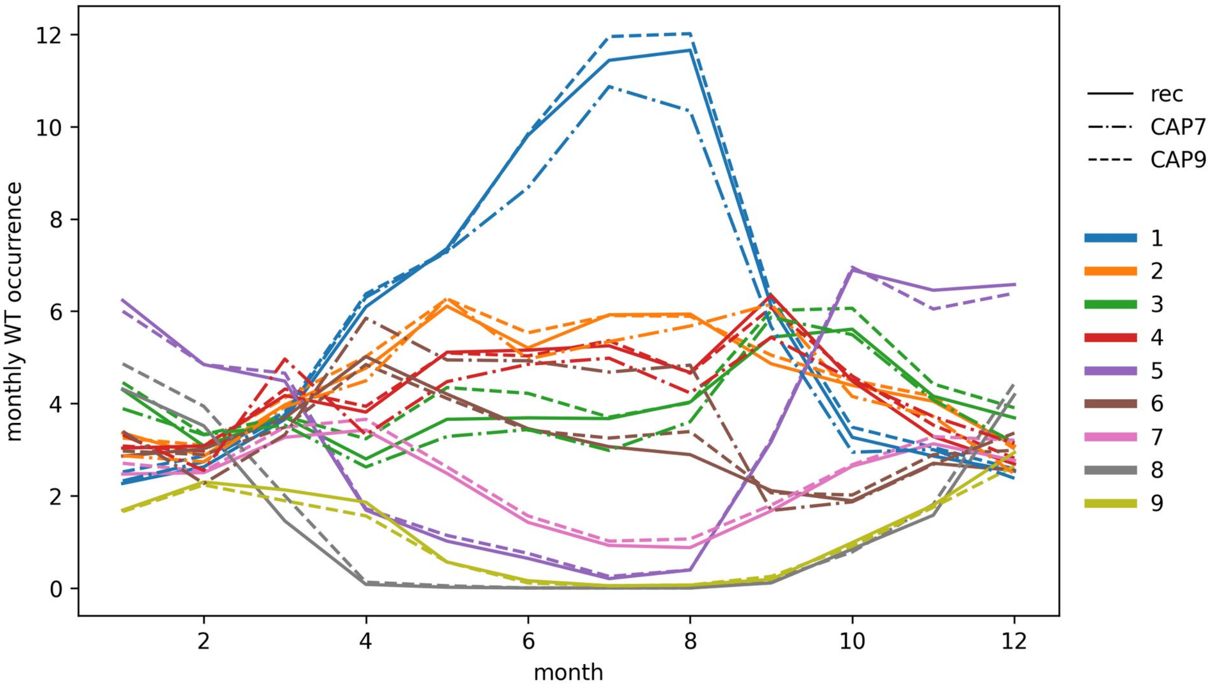

40 ***Figure S9:*** *average WT seasonality 1957–2020 for reference CAP9 series (dashed line), CAP9 reconstructions (solid lines), and CAP7 reconstructions (dash-dotted lines, Schwander et al., 2017).*

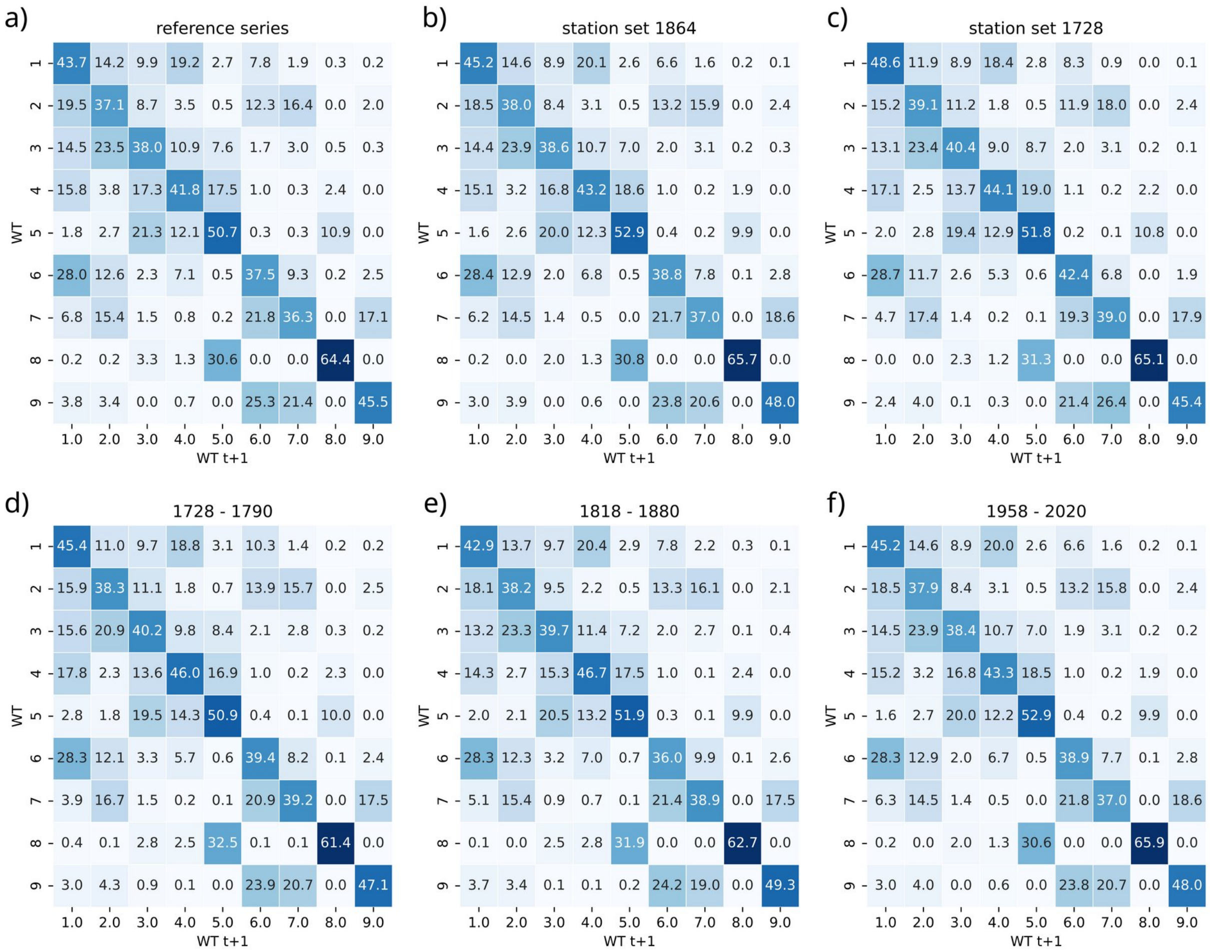

Figure S10: *preferential transitions between WTs from a given day (t, y-axis) to the following day (t+1, x-axis) in percent of days with the respective WT at time t. Indicated are preferential transitions for a) the reference series 1957–2020, b) the reconstructions with the 1864 station set (reference period 1957–2020), c) the reconstructions with the 1728 station set (reference period 1957–2020). Furthermore, d), e), and f) indicate the preferential paths in the indicated historical period of the CAP9 reconstructions.*

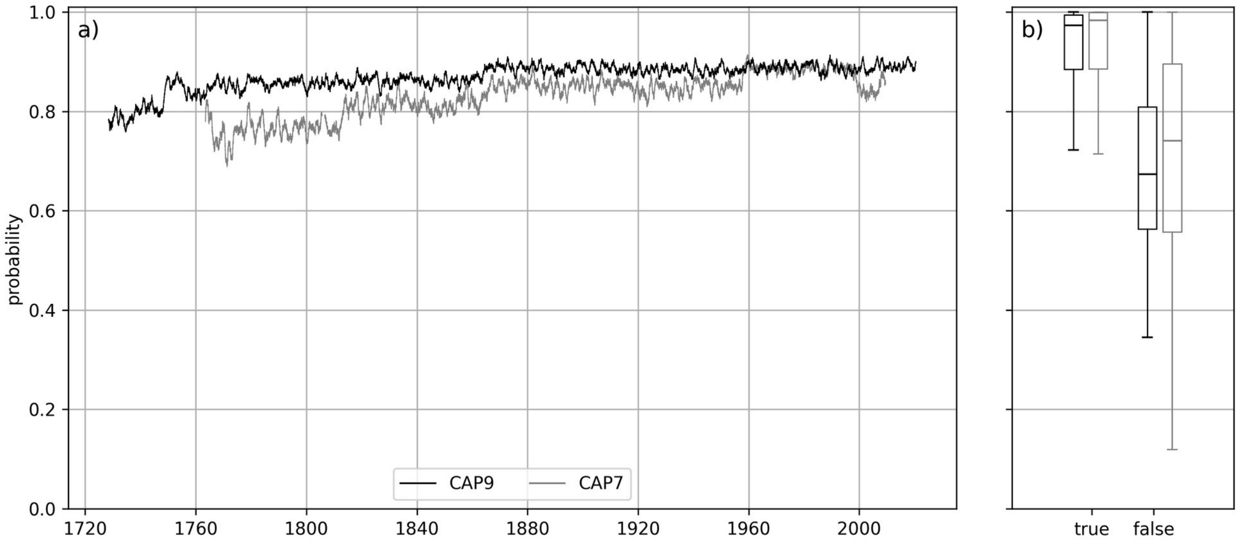

Figure S11: *a) 365–day running mean of the daily maximum probability (fraction) of the reconstructed CAP9 WT series (in black) and CAP7 WT series by Schwander et al. (2017) (in grey) and b) boxplots of the probability for correctly (true) and wrongly (false) attributed WTs within the reference period for the respective reconstructions.*

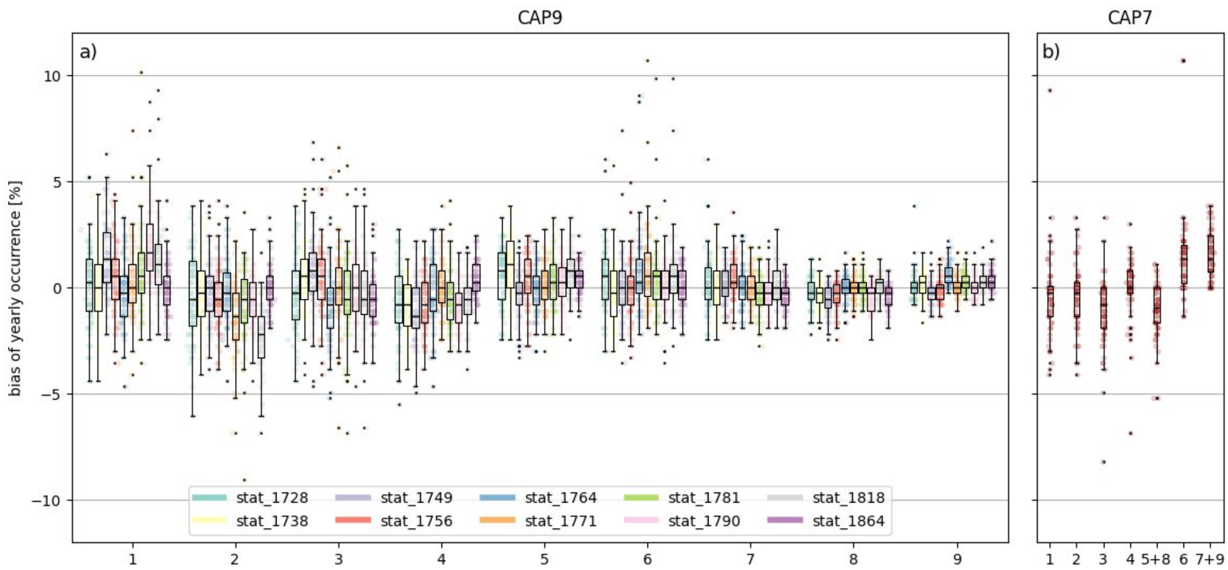

Figure S12: *Bias of yearly WT occurrence (in % of days) for all WTs (x–axis) and station sets (colors) in a) the NN reconstruction and b) the CAP7 dataset by Schwander et al. (2017).*

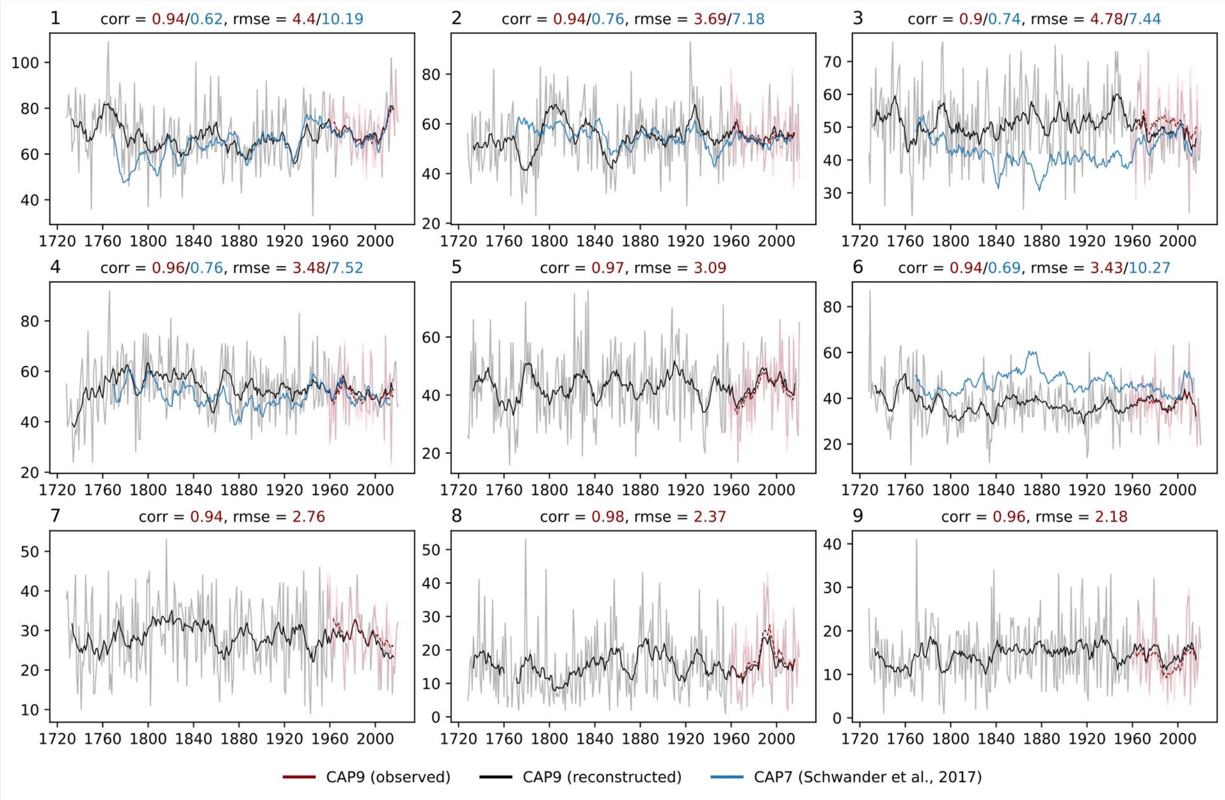

60 ***Figure S13 :*** *Yearly occurrence of reconstructed CAP9 WTs (lighter colors) with 10–year running mean (darker colors). Shown are the CAP9 reference series (red), the CAP9 reconstructions (black), and the CAP7 reconstructions (blue). Indicated are correlation and root mean squared error for the yearly WT occurrence with respect to the reference series.*

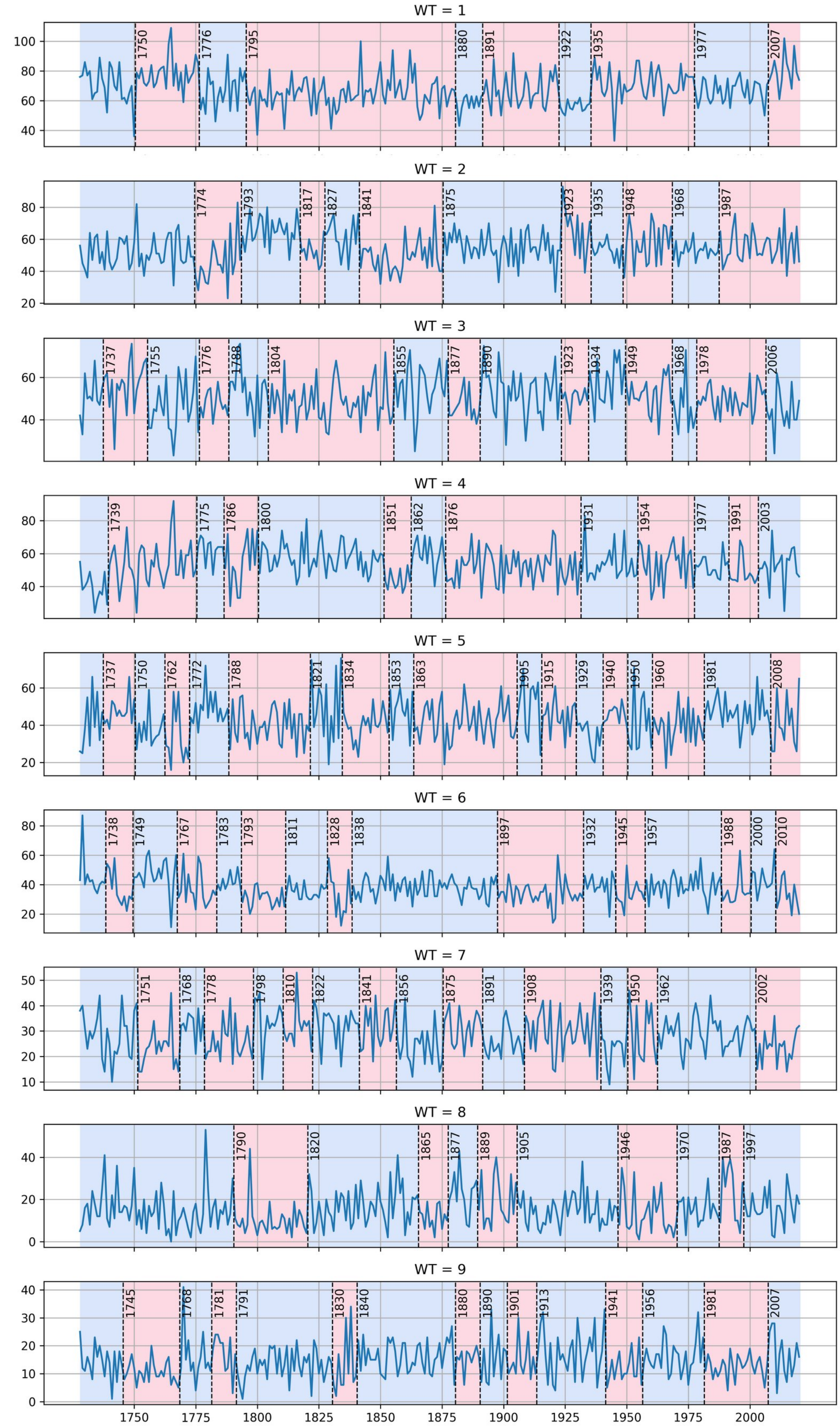

65 ***Figure S14 :*** *detected break points in the yearly WT occurrence of the CAP9 reconstructions using the PELT algorithm.*

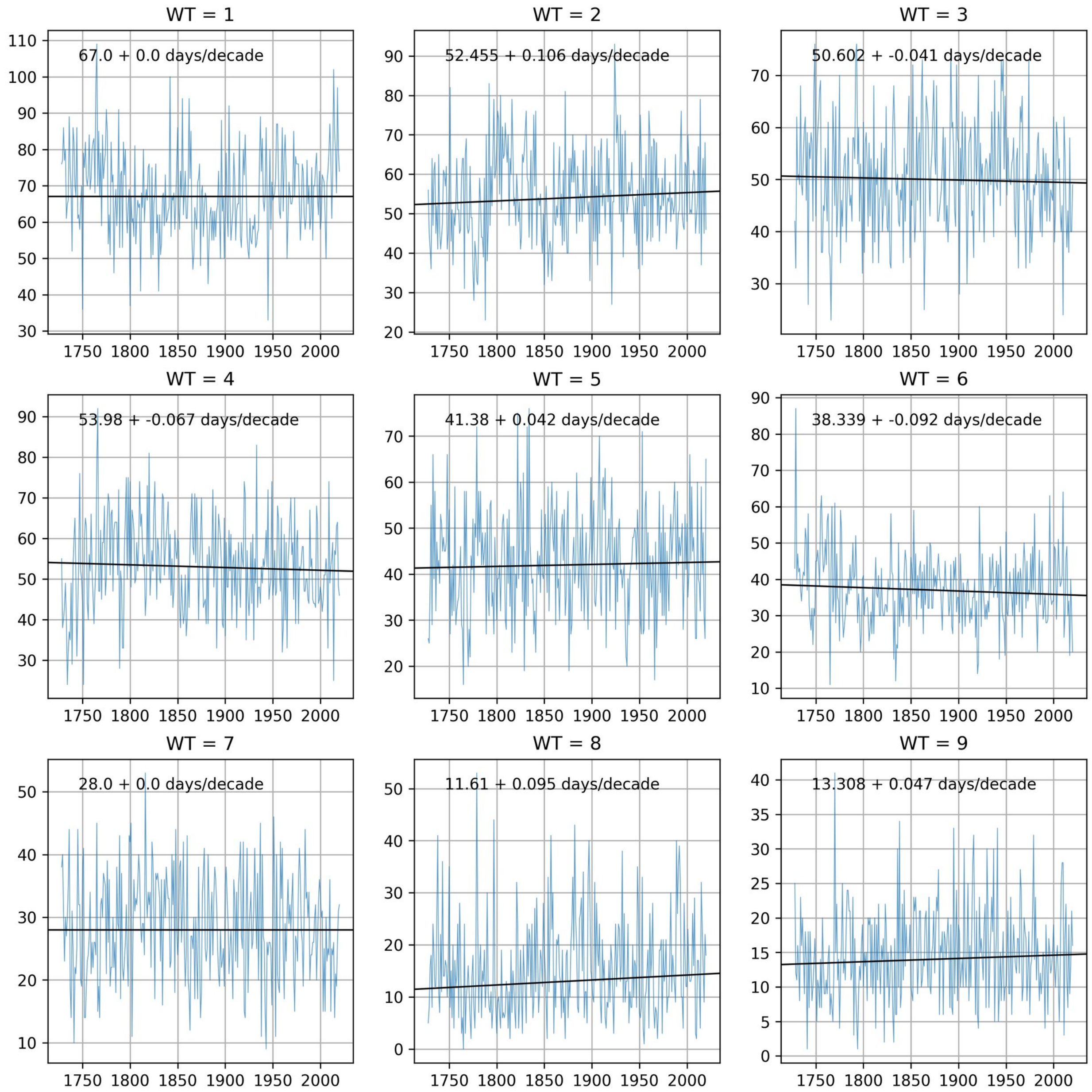

Figure S15: *trend estimates for yearly CAP9 WT occurrence in the reconstructed series. Asterisks indicate statistical significance for the Mann-Kendall trend test at a significance level of α = 0.05.*

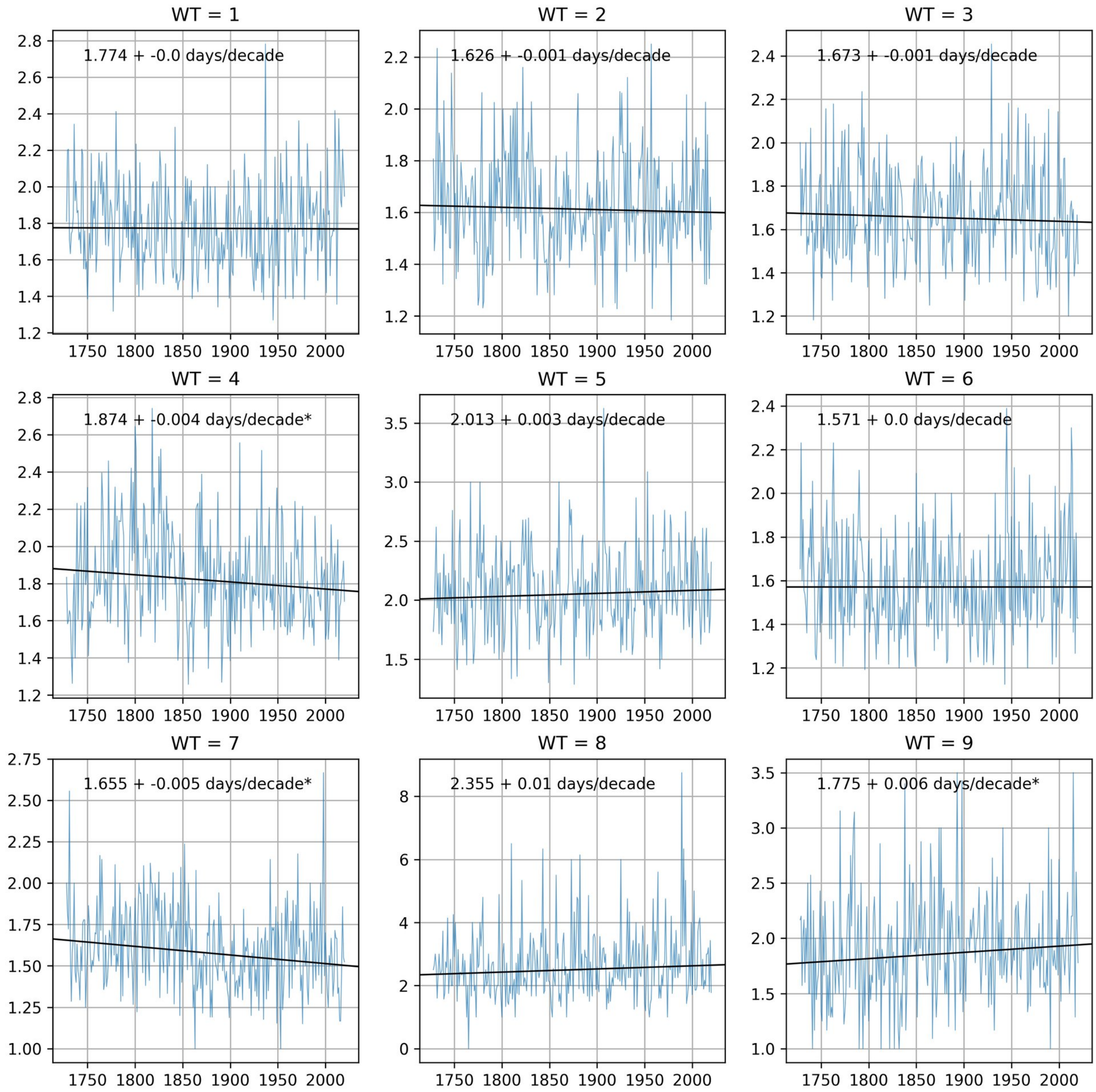

Figure S16: *trend estimates for yearly average CAP9 WT persistence in the reconstructed series. Asterisks indicate statistical significance for the Mann-Kendall trend test at a significance level of α = 0.05.*

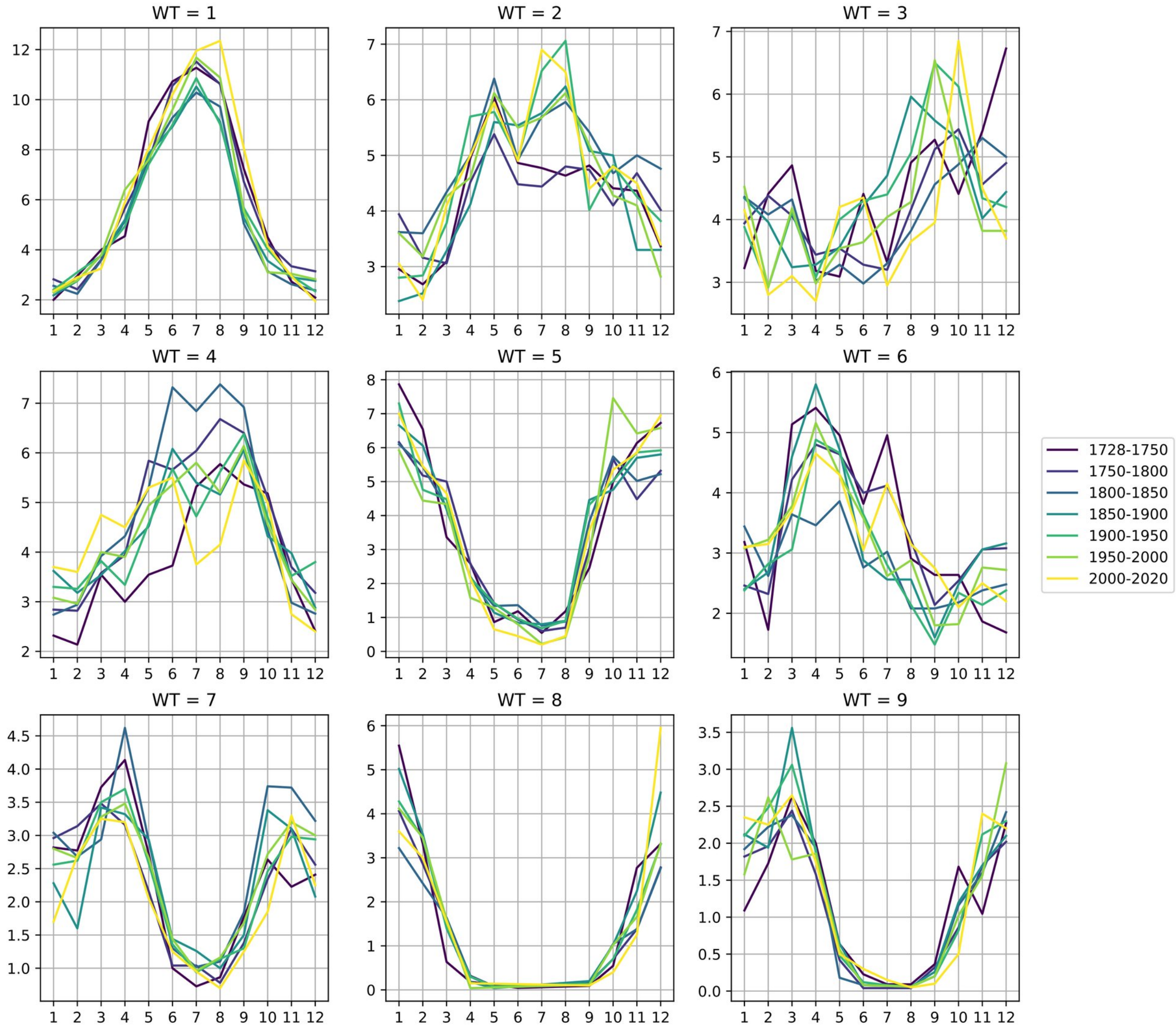

Figure S17 : *seasonal shifts of CAP9 WT occurrence in the reconstructed series. Indicated is the average monthly occurrence [days/month] for different periods (colors) indicated in the legend.*